COBEM 2023 27TH INTERNATIONAL CONGRESS OF MECHANICAL ENGENEERING

ABCM Brazilian Society of Mechanical Sciences and Engineering
27th ABCM International Congress of Mechanical Engineering
December 04-08, 2023, Florianópolis-SC, Brazil

COB-2023-0906
AERODYNAMIC STUDY OF THE USE OF A TELESCOPIC WINGLET IN AN AGRICULTURE AIRCRAFT

Daniel Valadares Roman de Paula
Joel Laguárdia Campos Reis
Federal University of Minas Gerais, Av. Pres. Antônio Carlos, 6627 - Pampulha, 6627, Belo Horizonte - Minas Gerais
danielvaladares10@ufmg.br, laguardia@demec.ufmg.br

João Paulo Eguea
University of São Paulo, Av. Trab. São Carlense, 400 - Parque Arnold Schimidt, São Carlos - São Paulo
joao.eguea@usp.br

Abstract. *Agricultural aircraft have proven to be important assets in a wide range of sectors due to their versatility. These aircraft are mostly used for crop spraying, which involves applying fertilizers, pesticides, and herbicides to crops. While on these flights, the aircraft frequently performs low-altitude maneuvers like wingovers that could place it in stall-threatened flight conditions. In this context, improving the aircraft's rate of climb using wingtip devices, particularly winglets, can be beneficial for the agriculture mission. These aerodynamic devices are employed to reduce the induced drag generated by wingtip vortices, which enhances lift and overall aircraft performance. In this sense, the purpose of this study is to evaluate the aerodynamic effects of the use of morphing telescopic winglet on agricultural aircraft through numerical simulations. The telescopic aspect of the winglet refers to its ability to expand or retract its only one moveable segment, producing a variable span. Doing so, the winglet can adjust its shape using this technology to accommodate different flight scenarios. The study utilizes a 3D Vortex-Lattice Method (VLM) to predict aerodynamic properties of a wing using two-dimensional airfoil characteristics. The research was conducted using an EMB-202 Ipanema wing-based model to investigate the effects of different winglet configurations on the aerodynamics and performance aspects of the aircraft. For this, a total of six winglet variants were investigated. These different winglet configurations were evaluated to verify if the variation of its span while in flight can improve the performance of the aircraft by reducing induced drag, enhancing operational safety, optimizing fuel efficiency, reducing emissions, and lowering overall operational costs.*

Keywords: *Agricultural Aircraft, Induced Drag, Winglet, Telescopic Winglet, Vortex-Lattice*

1. INTRODUCTION

Agricultural aircraft are vital for efficient cultivation, fire-fighting, and agricultural industry growth, making them crucial to the global economy. Prior comprehension of their significance is essential before exploring aerodynamic force predictions to enhance their design and performance. In this sense, this type of aircraft has proven to be an important asset in a wide range of sectors due to its versatility. The aircraft are mostly used for crop spraying, which involves applying fertilizers, pesticides, and herbicides to crops. While on these flights, the aircraft frequently performs low-altitude maneuvers like wingovers that could place it in stall-threatened flight conditions.

The capacity of altering the shape of a wing surface while in flight has been a topic of great interest for researchers and designers as it helps in minimizing the design trade-offs necessary. The task is to create a device that can withstand the specified forces while also having the ability to modify its form.

Moreover, this technique has an important use in agricultural aircraft, where the ability to change the wing shape while in flight can improve aerodynamic performance, and increase productivity in various agricultural operations. Increased precision and efficiency in agricultural operations are possible with the use of morphing devices in agricultural aircraft, which can improve the field's production.

One application of a morphing device that has never been applied to agricultural aircraft is the telescopic morphing winglet concept. The main work of this concept was carried by Samuel and Pines (2007) who designed, developed, and tested an unmanned aerial vehicle featuring a pneumatic telescoping wing that enables alteration in wingspan while maintaining aerodynamic wing loads. A complete version of the telescopic wing was constructed and also tested. The experiments involved conducting aerodynamic measurements at different Reynolds numbers.

The telescopic morphing concept had never been studied or applied to morphing winglets, despite all the research conducted on morphing winglets for aircraft. This was one of the motivations to pursue this study.

2. METHODOLOGY

The scope of this work was to study the aerodynamic and performance influence of adopting a telescopic winglet on a wing model based on the EMB-202 Ipanema wing. In this regard, six configurations were generated by varying the winglet's span. The telescopic feature of the winglet refers to its ability to expand or retract with only one movable segment, producing a variable span characteristic. Therefore, the different configurations were compared among themselves and mainly with the baseline Config1 configuration in the climb condition of the EMB-202 aircraft.

The wing and winglet airfoil employed in this study was the LAE-2319 developed by Professor Catalano and others at USP. This airfoil was used in many studies such as Bravo-Mosquera *et al.* (2018). Further, the airfoil coordinates were kindly provided by Professor Fernando Catalano and Professor João Paulo Eguea.

2.1 Telescopic winglet configurations

The baseline wing model used was based on the actual wing model that equips the EMB-202 aircraft developed by EMBRAER S.A., and on this study is referred as Config1, as shown in Figure 1(a). The other configurations were generated inspired by Samuel and Pines (2007). The methodology for generating the configurations was based on changing the winglet's span values while maintaining the cant angle value.

All configurations (Config1 to Config6) presented the geometric characteristics according to Table 1 and Table 2. Configurations Config2 to Config6 were obtained by varying the winglet span between 110% and 150% of the Config1 winglet's span. Furthermore, configurations 1 to 6 can be visualized in Figure 1.

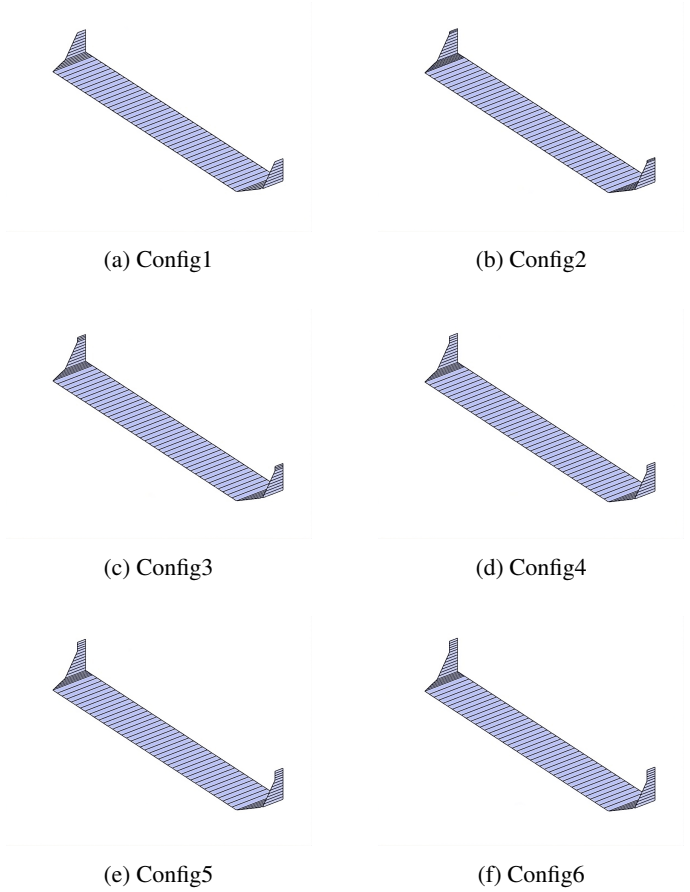

(a) Config1 (b) Config2

(c) Config3 (d) Config4

(e) Config5 (f) Config6

Figure 1: Configurations in the CEA-VLM environment.

2.2 Aerodynamic analysis

2.2.1 CEA-VLM

The selected aerodynamic analysis tool for this work is a 3D numerical procedure implemented in MATLAB, denoted CEA-VLM, and developed by de Vargas (2006). The two-dimensional calculation is performed based on external panel method. In this work, Xfoil was used to obtain the two-dimensional aerodynamic characteristics. The CEA-VLM method

Table 1: Wing geometric characteristics of each configuration.

Configuration	Wingspan	Wing's chord	Number of panels
Config1	11.2	1.715	25
Config2	11.2	1.715	27
Config3	11.2	1.715	26
Config4	11.2	1.715	26
Config5	11.2	1.715	26
Config6	11.2	1.715	26

(1) Dimension in meters (m).

Table 2: Winglet geometric characteristics of each configuration.

Configuration	Winglet's root chord	Winglet's tip chord	Winglet's span	Number of panels
Config1	0.53	0.35	0.880	8
Config2	0.53	0.35	0.968	10
Config3	0.53	0.35	1.056	11
Config4	0.53	0.35	1.144	11
Config5	0.53	0.35	1.232	12
Config6	0.53	0.35	1.320	13

(1) Dimension in meters (m).

is employed to estimate the aerodynamic properties of airfoils and wing-tail combinations in the subsonic regime. As for the three-dimensional calculation, the procedure estimates the aerodynamic characteristics based on the locally effective angle of attack and local airfoil data. This method is capable of calculating the forces and moments (and therefore also the coefficients and derivatives) of wing-tail combinations in practically any flight condition in the subsonic regime.

The CEA-VLM is a variant of the Vortex-lattice method based on the Weissinger (1947) method. While both methods discretize the flow field and determine the vortex circulation using a lattice structure, the Weissinger method is more of a refinement of the Lifting line theory and incorporates different singularities. In order to improve the accuracy and application of the method in comparison to a standard VLM, these improvements may include more precise wake modeling, handling of unsteady flows, taking compressibility effects into account, or other modifications. In this sense, the CEA-VLM was used in this work because it is a recommended method for solving typical problems in subsonic aircraft design, which fits the types of missions of the aircraft, and because it has a low computational cost.

2.3 Performance analysis

2.3.1 Climb condition

Agricultural aircraft is often engaged in low-altitude maneuvers like wingovers during its flights, placing it in potential stall-threatened conditions. Given these operational circumstances, the climb condition was identified as the most suitable phase to evaluate the telescopic winglet.

In this way, according to the requirements specified in FAR 23 for climb performance in normal, utility, and acrobatic categories (FAR 23.67 b1) and as mentioned in the work by Roskam and Lan (1997), an aircraft with reciprocating power and a maximum takeoff weight ($W_{TO_{max}}$) of up to 2721.55 kg, and a stall speed (V_S) of up to 118.57 m/s, must adhere to the speed limitations outlined in Eq.(1).

$$V_{cl} \geq 1.25 \times (V_s) \tag{1}$$

According to the reports by Comando da Aeronáutica (2023) and Comando da Aeronáutica (2019), for the EMB-202 Ipanema aircraft in the restricted category with reciprocating power, having a maximum takeoff weight ($W_{TO_{max}}$) of 2721.55 kg and a stall speed (V_S) of 27.72 m/s (flaps retracted), the following information can be derived:

$$V_{cl} \geq 1.25 \times (27.72) = 34.65 m/s \tag{2}$$

Where,

$$V_{cl} = 34.65 m/s \tag{3}$$

Thus, a speed of 34.65 m/s was used representing the aircraft climb condition.

Additionally, according to Nicks (1983), the aerodynamic parameter ($C_L^{3/2}/C_D$) is pivotal in determining the rate of climb (RC) of an aircraft: the higher its value, the greater the rate of climb of the aircraft. This parameter, in conjunction with the maximum (C_L), plays a crucial role in the performance during takeoffs, go-arounds, and wingovers. Therefore, this parameter has been chosen to compare different configurations of the aircraft. Its significance can be indirectly measured and analysed by Eq. (4).

$$RC \propto \frac{C_L^{3/2}}{C_D} \tag{4}$$

2.4 Simulation environment (CEA-VLM)

Simulations were carried out in CEA-VLM for each configuration described and their respective geometric boundary conditions under climb flight condition. The type of mesh chosen for the analysis was a linear distribution in all sections of the wing and winglet as shown in Figure 1. This type of distribution was chosen over others because when testing the other types of meshes offered by CEA-VLM, such as sinusoidal and cosineoidal, the linear distribution already presented results in convergence.

The number of panels for each section were determined using an iterative mesh refinement method, as shown in Table 1 and Table 2. This approach involved initially testing a coarse mesh and progressively increasing the number of panels while assessing the improvement in outputs. The final selection of the panel count was based on result convergence, where the number of panels for each wing section was chosen to achieve satisfactory results, ensuring that further mesh refinement did not yield significant improvements.

It is important to acknowledge that working with discontinuous geometries with the CEA-VLM routine that was used can lead to errors in the outputs. Thus, in order to generate a trapezoidal winglet with a root chord smaller than that of the base wing, it was necessary to create a trapezoidal transition surface that connected the end of the base wing to the beginning of the winglet in order to obtain the design value of the root chord of the Ipanema's winglet, as shown in Figure 1. In other words, a geometric approximation was made to work around the geometric discontinuity limitation of CEA-VLM routine. Moreover, it is important to emphasize that it was known that using this type of transition surface could generate inaccuracies in the results.

2.5 Data analysis and discussion

The data analysis applied in this work was a methodology already employed in other works such as Coimbra and Catalano (1999), Cerón-Muñoz and Catalano (2006), Cosin *et al.* (2010), Céron-Muñoz *et al.* (2013), Bravo-Mosquera *et al.* (2018), Eguea *et al.* (2018), Panagiotou *et al.* (2018), Eguea (2019), Ryseck *et al.* (2019), Eguea *et al.* (2020), Guerrero *et al.* (2020), Eguea *et al.* (2021), and Panagiotou *et al.* (2022).

It is a parametric analysis and consists of obtaining the aerodynamic coefficients of lift and drag as a function of the angle of attack and/or lift coefficient through experiments or numerical tools. These components are obtained for each wing configuration studied, i.e., the parameters of the geometric boundary conditions are varied through the application of morphing devices. In the case of this work, the analyzed device was the telescopic winglet for an agricultural aircraft.

From the above data, the lift coefficient is studied as a function of the angle of attack. The total drag and induced drag coefficients are analyzed as a function of the lift coefficient. In addition, a study of performance parameters is also carried out. Thus, the parameter ($C_L^{3/2}/C_D$), proportional to the rate of climb, is analyzed. The aerodynamic study aims to indicate improvements in performance parameters from the use of the telescopic winglet.

3. RESULTS AND DISCUSSION

To establish the range of C_L for the climb condition, Figure 5(a) was used to determine an optimized range close to $(C_L^{3/2})/(C_D)_{max}$. As a result, the defined range for analysis was set as $0.64 \leq C_L \leq 1.35$.

3.1 Aerodynamic analysis

3.1.1 Lift coefficient

According to Table 3, Figure 2(a) and Figure 2(b), it can be inferred that as the telescopic winglet extension is activated, the configurations assume increasingly higher values of ($\partial C_L/\partial\alpha$). These values of ($\partial C_L/\partial\alpha$) with respect to Config1 showed progressively larger results. These results are better visualized through the bar charts in Figure 2(c) and Figure 2(d). It is important to note that the percentage values in Table 3 are relative to Config1.

Moreover, Config6 obtained the largest increase in $\partial C_L/\partial\alpha$ (+0.7379%) and $C_{L_{max}}$ (+0.6748%) when compared to Config1, as shown in Figure 2(c) and Figure 2(d). In this sense, activating the telescopic winglet extension during the climb regime has shown to have discreet performance gains in terms of $\partial C_L/\partial\alpha$ and $C_{L_{max}}$, which was expected.

Table 3: CEA-VLM simulation results.

Parameter	Config1	Config2	Config3	Config4	Config5	Config6
$\partial C_L/\partial\alpha$	0.07618	0.07634	0.07647	0.07658	0.07667	0.07674
% $\partial C_L/\partial\alpha$	-	+0.2094	+0.3823	+0.5244	+0.6389	+0.7379
$C_{L_{max}}$	1.5857	1.5884	1.5928	1.5942	1.5954	1.5964
α for $C_{L_{max}}$	21°	21°	21°	21°	21°	21°
% $C_{L_{max}}$	-	+0.1703	+0.4477	+0.5360	+0.6117	+0.6748
C_D for $C_L = 0.72$	0.02743	0.02713	0.02684	0.02658	0.02634	0.02613
% C_D for $C_L = 0.72$	-	-1.1091	-2.1522	-3.1293	-3.9917	-4.7611
C_{D_i} for $C_L = 0.72$	0.02110	0.02075	0.02042	0.02010	0.01984	0.01962
% C_{D_i} for $C_L = 0.72$	-	-1.6697	-3.2146	-4.7558	-5.9686	-7.0151
C_D for $C_L = 0.98$	0.04677	0.04708	0.04627	0.04577	0.04586	0.04551
% C_D for $C_L = 0.98$	-	+0.6940	-1.05138	-2.1169	-1.9258	-2.6829
C_{D_i} for $C_L = 0.98$	0.03887	0.03835	0.03778	0.03726	0.03687	0.03646
% C_{D_i} for $C_L = 0.98$	-	-1.3431	-2.8212	-4.1349	-5.1485	-6.1996
$(C_L^{3/2}/C_D)_{max}$	22.2690	22.5177	22.7650	22.9942	23.2027	23.3947
C_L for $(C_L^{3/2}/C_D)_{max}$	0.7190	0.7209	0.7225	0.7238	0.7249	0.7259
% $(C_L^{3/2}/C_D)_{max}$	-	+1.1168	+2.2273	+3.2565	+4.1928	+5.0550

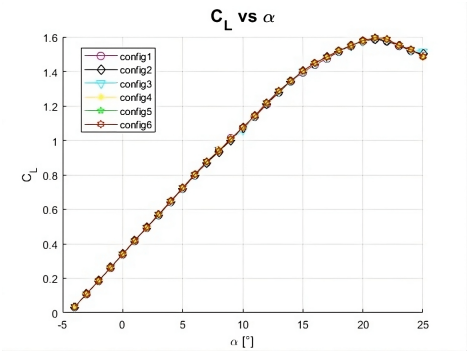

(a) Lift coefficient vs. α

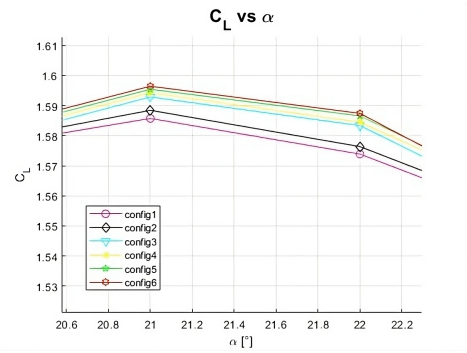

(b) Lift coefficient vs. α at stall region

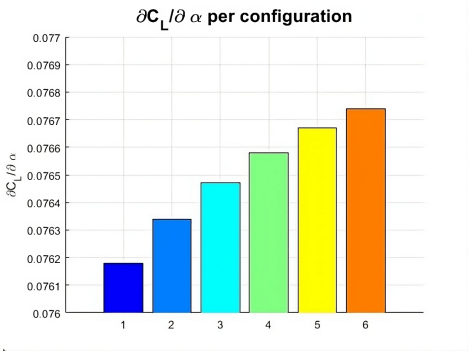

(c) Lift coefficient slope

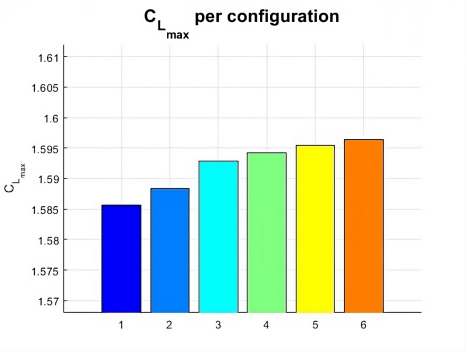

(d) Maximum lift coefficient

Figure 2: Lift coefficient analysis.

3.1.2 Drag coefficient

Due to inaccuracies in the implementation of the aerodynamic model, there is a significant degree of uncertainty in predicting drag using VLM simulations. Therefore, accurately evaluating the total drag and induced drag of the configurations is very challenging, as demonstrated in Figure 3(a) and Figure 4(a).

For this part, two points within the interval $0.64 \leq C_L \leq 1.35$ were first analyzed with the aim of studying the behavior of total and induced drag. The first chosen point was $C_L = 0.72$ because it represents, according to Figure 5(a), the average value of $(C_L^{3/2}/C_D)_{max}$ for all configurations. In other words, it represents the value of an optimal climb for

the aircraft. In addition, $C_L = 0.98$ was also analyzed as it represents the average value of the interval $0.64 \leq C_L \leq 1.35$ and it does not represent an optimal climb value, which is closer to reality.

For $C_L = 0.72$, according to Table 3, as the telescopic winglet was extended through configurations Config2 to Config6, it can be seen that the induced drag coefficient decreased, with a notable decrease of -7.0151% through Config6. Similarly, the total drag coefficient also decreased according to Table 3, with the decrease of -4.7611% in Config6 also standing out.

However, an interesting result obtained was that the total drag and induced drag coefficients did not show equal or at least similar rates of decrease in order of magnitude. For example, while the drag coefficient of Config6 decreased by -4.7611%, the induced drag coefficient of the same configuration decreased by -7.0151%. Thus, these unequal rates of decrease could indicate an increase in other types of drag in the parasitic drag component of the total drag.

For $C_L = 0.98$, according to Table 3, in the same way, it is possible to see that the induced drag coefficient decreased, with a notable decrease of -6.1996% through Config6. Similarly, the total drag coefficient also decreased according to Table 3, with the decrease of -2.6829% in Config6 also standing out. These unequal rates of decrease again indicate an increase in other types of drag in the parasitic drag component of the total drag.

However, for $C_L = 0.98$, another interesting result was that when activating Config2, the parasitic drag component of the total drag increased significantly, resulting in an increase of the total drag coefficient by +0.6940%. Besides this fluctuation, when activating Config5, the total drag coefficient also presents a counter trend of growth, but more subtle. In addition to Table 3, the results discussed here in absolute values can be visualized in Figure 3(b), Figure 3(c), Figure 4(b), and Figure 4(c).

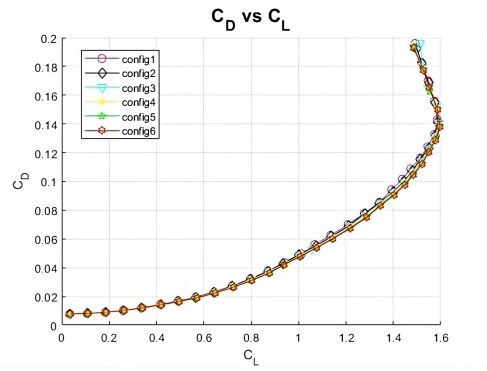

(a) Drag coefficient vs. Lift coefficient

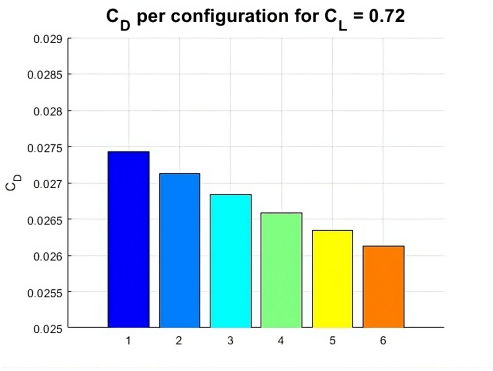

(b) Drag coefficient at $C_L = 0.72$

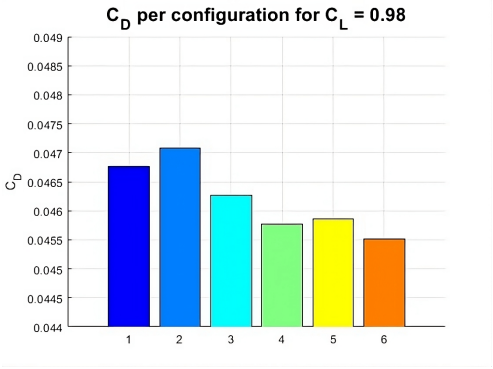

(c) Drag coefficient at $C_L = 0.98$

Figure 3: Drag coefficient analysis.

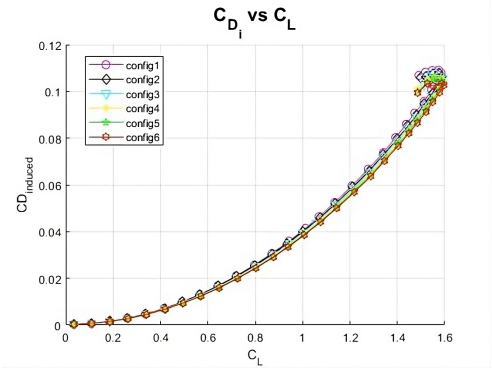

(a) Induced drag coefficient vs. Lift coefficient

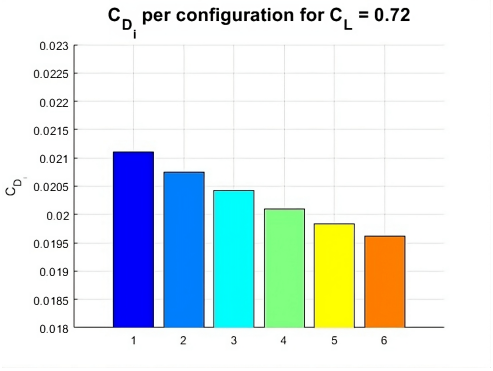

(b) Induced drag coefficient at $C_L = 0.72$

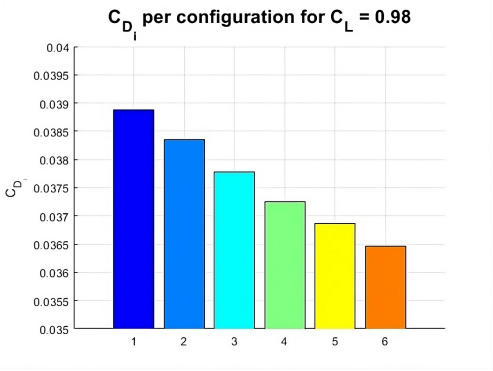

(c) Induced drag coefficient at $C_L = 0.98$

Figure 4: Induced drag coefficient analysis

3.2 Performance analysis

3.2.1 Rate of climb

The optimization of the performance parameter rate of climb is considered the most important for agricultural applications since during typical missions, the aircraft is put in flight situations where it performs maneuvers such as the wingover and procedures such as go-arounds, which require high aerodynamic performance through the generation of lift in flight conditions close to the wing stall (low speed and high angle of attack).

The increase in rate of climb $(C_L^{3/2})/(C_D)$ was observed through Figure 5(a) with the adoption of extension of the telescopic winglet (Config2 to Config6) in the climb range ($0.64 \leq C_L \leq 1.35$), compared to Config1. The maximum increment in $(C_L^{3/2})/(C_D)_{max}$ was found when activating Config6, with $(C_L^{3/2})/(C_D)_{max} = 23.3947$, which represents an increment of +5.0550% compared to Config1. The results can be better visualized through the bar chart shown in Figure 5(d) and the corresponding data can be found in Table 3. In the same manner, this parameter showed a similar behavior throughout the entire climb interval. That is, extending the telescopic winglet by adopting the configuration formats Config2 to Config6 proved to be aerodynamically beneficial. However, there were few exceptions that must be analyzed.

Between the interval $0.86 \leq C_L \leq 1.16$, there were some performance exchanges among the configurations. To facilitate analysis, this interval was divided into two, the first being $0.86 \leq C_L < 1$ and the second $1 \leq C_L \leq 1.16$, according to Figure 5(b) and Figure 5(c).

For the first interval ($0.86 \leq C_L < 1$), for C_L close to 0.94, Config1 performed better than Config2, meaning that not extending the telescopic winglet to the second configuration was more advantageous. However, Config3 and Config4 showed better performance among the configurations for C_L close to 0.94. This represents an advantage in terms of aerodynamic load as extending configurations with smaller wingspan (compared to Config5 and Config6) can be beneficial in terms of a possible increase in bending moment at the wing root. However, for this point, Config4 presented a gain in $(C_L^{3/2})/(C_D)$ compared to Config6 of only 1%.

For the second interval ($1 \leq C_L \leq 1.16$), for C_L close to 1.06, Config3 performed similarly to the Config5, which again represents an advantage in relation to aerodynamic loads. In this sense, extending Config3 instead of Config4 and Config5 becomes more interesting.

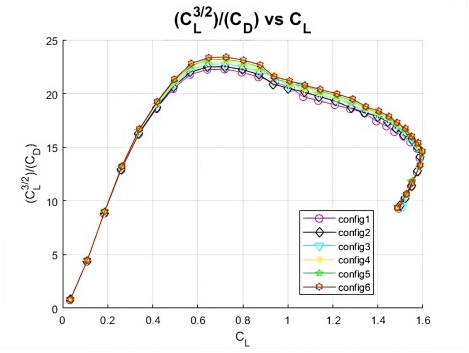

(a) $(C_L^{3/2})/(C_D)$ vs. Lift coefficient

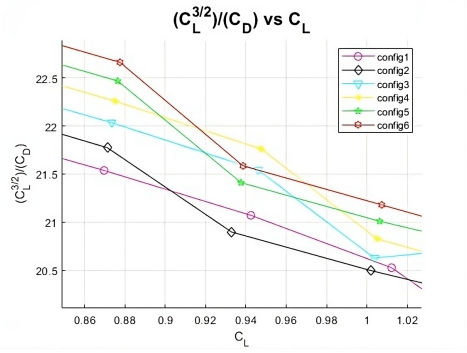

(b) $(C_L^{3/2})/(C_D)$ vs. C_L at First Exception

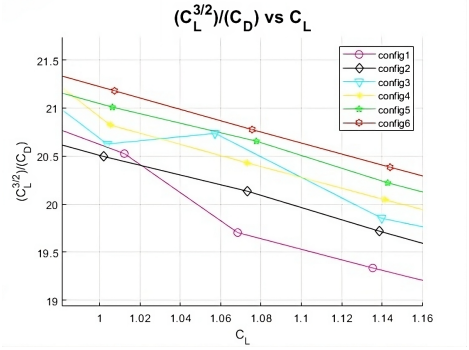

(c) $(C_L^{3/2})/(C_D)$ vs. C_L at Second Exception

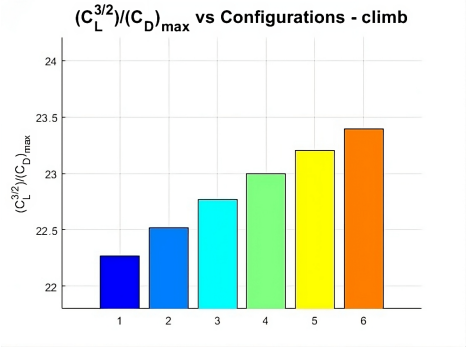

(d) $(C_L^{3/2})/(C_D)_{max}$

Figure 5: Rate of climb parameter analysis.

4. CONCLUSION

The telescopic winglet extension leads to higher values of $\partial C_L/\partial\alpha$ and results in progressively larger increases compared to Config1. Config6 exhibits the largest improvements in $\partial C_L/\partial\alpha$ (+0.7379%) and $C_{L_{max}}$ (+0.6748%) when compared to Config1. Activating the telescopic winglet extension during the climb regime demonstrates discrete performance gains as anticipated.

In terms of induced drag, the adoption of a telescopic winglet initially appears positive because this parameter showed decreasing rates as the winglet was activated. On the other hand, there was an indication of an increase in total drag, which represents a tradeoff in adopting the telescopic winglet.

The gains in $(C_L^{3/2})/(C_D)_{max}$ through the adoption of Config2 to Config6 demonstrated positive outcomes for the agricultural mission of the aircraft. The parameter $(C_L^{3/2})/(C_D)_{max}$ increased with the extended telescopic winglet from Config2 to Config6 in the climb range compared to Config1. Config6 exhibited the most significant enhancement with $(C_L^{3/2})/(C_D)_{max} = 23.3947$, representing a +5.0550% increase over Config1.

For the rate of climb parameter $(C_L^{3/2})/(C_D)$, in the first interval ($0.86 \leq C_L < 1$), Config1 outperformed Config2 for C_L close to 0.94, while Config3 and Config4 showed superior performance. Configurations with smaller wingspan demonstrated advantages in terms of aerodynamic load and potential bending moment increase at the wing root. Config4 exhibited a slight gain in $(C_L^{3/2})/(C_D)$ compared to Config6.

In the second interval ($1 \leq C_L \leq 1.16$), Config3 performed similarly to Config5, indicating an advantage in aerodynamic loads. Extending Config3 becomes a more favorable option compared to Config4 and Config5. Overall, the optimal winglet configuration depends on specific flight conditions and the trade-off between aerodynamic load benefits and potential wing root bending moments.

Despite the performance variations observed among the configurations in the desired C_L range, they were very discreet (on the order of only 1%). In other words, considering the error margin of the CEA-VLM method used in this study, it can be concluded that the performance gains are not realistic.

Based on this study, the telescopic winglet's efficacy in the Ipanema aircraft's climb range is limited, with few exceptions. Preliminary results indicate a fixed winglet, especially configurations beyond Config1, might be preferable. However, more research is needed in this domain. Future investigations should assess the robustness and reliability of telescopic winglets, focusing on vibrations, flutter, and flight quality. Utilizing CFD simulations and wingtip vortex visu-

alization will elucidate their aerodynamic behavior under diverse flight conditions. Direct bending moment measurements at the wing root are crucial for understanding structural and aerodynamic integrity. Further, optimizing fuel savings in agricultural tasks and winglet activation enhances their real-world applicability and efficiency.

5. REFERENCES

Bravo-Mosquera, P.D., Cerón-Muñoz, H.D., Díaz-Vázquez, G. and Catalano, F.M., 2018. "Conceptual design and cfd analysis of a new prototype of agricultural aircraft". *Aerospace Science and Technology*, Vol. 80, pp. 156–176.

Cerón-Muñoz, H.D. and Catalano, F.M., 2006. "Experimental analysis of the aerodynamic characteristics adaptive of multi-winglets". *Proceedings of the Institution of Mechanical Engineers, Part G, Journal of Aerospace Engineering*, Vol. 220, pp. 209–215.

Coimbra, R.F. and Catalano, F.M., 1999. "An experimental study on wingtip devices for agricultural aircraft". In *Proceedings of the 22th Congress of the International Council of the Aeronautical Sciences*. Member Societies and Executive Committee, Conference Centre, United Kingdom.

Comando da Aeronáutica, A., 2023. "EspecificaÇÃo de tipo nº ea-7104". ANAC, São José dos Campos, sistemas.anac.gov.br/certificacao/Produtos/EspecificacaoDetail.asp?CHTCodi=7104. Accessed 26 Oct 2023.

Comando da Aeronáutica, C., 2019. "A-032/cenipa/2019 pt-vuu". CENIPA, Brasília, gov.br/anac/pt-br/assuntos/seguranca-operacional/gerenciamento-da-seguranca-operacional/relatorio-de-acidentes/arquivos/2019/. Accessed 26 Oct 2023.

Cosin, R., Catalano, F., Correa, L. and Entz, R., 2010. "Aerodynamic analysis of multi-winglets for low speed aircraft". In *Proceedings of the 27th International Congress of the Aeronautical Sciences*. Member Societies and Executive Committee, Nice, France.

Céron-Muñoz, H.D., Cosin, R., Coimbra, R.F.F., Correa, L.G.N. and Catalano, F.M., 2013. "Experimental investigation of wing-tip devices on the reduction of induced drag". *Journal of Aircraft*, Vol. 50, pp. 441–449.

de Vargas, L.A.T., 2006. *Desenvolvimento e implementação de um procedimento numérico para cálculo de conjuntos asa-empenagens de geometria complexa em regime de vôo subsônico, assimétrico e não linear*. Master's thesis, Master Program in Mechanical Engineering, Federal University of Minas Gerais, Belo Horizonte, Brasil.

Eguea, J.P., Bravo-Mosquera, P.D. and Catalano, F.M., 2021. "Camber morphing winglet influence on aircraft drag breakdown and tip vortex structure". *Aerospace Science and Technology*, Vol. 119, p. 107148.

Eguea, J.P., Catalano, F.M., A, A.M., Santana, L.D., Venner, C.H. and Silva, A.L.F., 2018. "Study on a camber adaptive winglet". In *Proceedings of the 2018 Applied Aerodynamics Conference*. American Institute of Aeronautics and Astronautics, Atlanta, United States.

Eguea, J.P., Silva, G.P.G. and Catalano, F.M., 2020. "Fuel efficiency improvement on a business jet using a camber morphing winglet concept". *Aerospace Science and Technology*, Vol. 96, p. 105542.

Eguea, J.P., 2019. *Genetic optimization and experimental validation of a camber morphing winglet*. Master's thesis, Master Program in Aeronautical Engineering, University of São Paulo, São Paulo, Brasil.

Guerrero, J.E., Sanguineti, M. and Wittkowski, K., 2020. "Variable cant angle winglets for improvement of aircraft flight performance". *Meccanica*, Vol. 55, pp. 1917–1947.

Nicks, O., 1983. "Wing extensions for improving climb performance". In *Aircraft Design, Systems and Technology Meeting*. American Institute of Aeronautics and Astronautics, Fort Worth, United States.

Panagiotou, P., Antoniou, S. and Yakinthos, K., 2022. "Cant angle morphing winglets investigation for the enhancement of the aerodynamic, stability and performance characteristics of a tactical blended-wing-body uav". *Aerospace Science and Technology*, Vol. 123, p. 107467.

Panagiotou, P., Efthymiadis, M., Mitridis, D. and Yakinthos, K., 2018. "A cfd-aided investigation of the morphing winglet concept for the performance optimization of fixed-wing male uavs". In *Proceedings of the 2018 Applied Aerodynamics Conference*. American Institute of Aeronautics and Astronautics, Atlanta, United States.

Roskam, J. and Lan, C.T.E., 1997. *Airplane aerodynamics and performance*. DARcorporation, St, Lawrence, United States.

Ryseck, P., Yeo, D., Hrishikeshavan, V. and Chopra, I., 2019. "Aerodynamic and mechanical design of a morphing winglet for a quadrotor biplane tail-sitter". In *Proceedings of the Vertical Flight Society 8th Autonomous VTOL Symposium*. Vertical Flight Society, Mesa, United States.

Samuel, J.B. and Pines, D., 2007. "Design and testing of a pneumatic telescopic wing for unmanned aerial vehicles". *Journal of Aircraft*, Vol. 44, pp. 1088–1099.

Weissinger, J., 1947. "The lift distribution of swept-back wings". NASA, Washington, https://ntrs.nasa.gov/citations/20030064148. Accessed 26 Oct 2023.

6. RESPONSIBILITY NOTICE

The authors are solely responsible for the printed material included in this paper.